IEEE Access
Multidisciplinary | Rapid Review | Open Access Journal

Received January 11, 2022, accepted January 28, 2022, date of publication March 29, 2022, date of current version May 3, 2022.

Digital Object Identifier 10.1109/ACCESS.2022.3149009

Torque Characteristics Analysis of a Novel Hybrid Superconducting Magnetic Coupling With Axial-Flux Using a Magnetic Equivalent Circuit Model

BORIS JOEL KENNE TELEZING, CHAOJUN YANG, PATRICK DJOMO OMBOLO, ZHIZHUO PENG, JIANGXI TAI, AND LI ZHU
School of Mechanical Engineering, Jiangsu University, Zhenjiang 212013, China

Corresponding author: Chaojun Yang (yangchaojun@ujs.edu.cn)

This work was supported in part by the National Natural Science Foundation of China under Grant 51875254, and in part by the Six Talent Peak Projects of Jiangsu Province under Grant 2015-ZBZZ-020.

ABSTRACT A novel hybrid superconducting coupling (NHSC) is proposed in this paper, in which the secondary is composed of copper and a split superconductor. A magnetic equivalent circuit (MEC) model is presented to analyze and calculate the distribution of the magnetic field and torque characteristics. The 3D modeling considers the end effects encountered in mating. The expressions of the magnetic flux and torque are obtained by combining Kirchhoff's law and Ampere's loop law, respectively. A 3D finite element (FE) model is built, and the simulation is performed. Its performance is investigated using a 135K critical high-temperature superconductor to have a greater operating margin of the coupling. For a high slip speed of 1500 rpm, we observed a peak torque of 167 Nm and stability of 115 Nm. By varying the thickness of the air gap or the PMs, we observed the increasing or decreasing of the torque. Due to the cryogenics systems, we also observed the reduction of the losses by the joule effect. The maximum error between the results of the torque obtained by simulation and the results calculated using the proposed model is 6.74%, which proves that both results are in good agreement.

INDEX TERMS Hybrid superconducting magnetic coupling, magnetic equivalent circuit (MEC), split superconductor disk, torque.

I. INTRODUCTION

Eddy-current couplings are becoming popular devices for speed-control and torque-control. They are very useful in applications requiring the transmission of motion between two environments with different atmospheres [1]–[4]. The efficiency of these couplings depends on the excitation level. The absence of mechanical contact allows a significant increase in the life of the coupling. In addition, the nature of the torque transmission provides intrinsic protection against mechanical overload [5]. To transmit torque without contact, [3] studied an eddy current coupling where the primary disc was composed of PMs and the secondary disc was equipped with the conductor. This eddy current coupling was effective but the transmitted torque was not large enough, where [6] studied an eddy current coupling with a slotted disk. The slotted conductor disk was composed of the conductor disk with slot cuts, that facilitate the flow of currents inappropriate routes to avoid stray currents and therefore to improve the torque. The latter in turn fails or presents weaknesses when it comes to the production of high torque, high speed, and present substantial damping at high speed. With the existence of resistance at the conductor disk, we can also have losses by Joules effect. In the context of minimizing or even eradicating these problems mentioned above, superconductors were proposed [7].

The associate editor coordinating the review of this manuscript and approving it for publication was Xiaodong Liang.

II. BACKGROUNG AND HISTORY

Several researchers [8]–[12] have studied different superconducting materials, and their critical temperature limit

and speed transmission characteristics, but mainly focused on direct current induction heaters, maglev trains, and wires [7]–[10]. [13]–[14] discovered a superconducting material at room temperature, a carbon hydride, and sulfur, Tc = 287.7 ± 1.2 K (about 15 °C), but under a pressure of 267 ± 10 GPa (close to the pressure at the center of the Earth). Based on the superconductor and its critical temperature [15], a superconducting coupling device is developed to transmit torque without contact. However, it could solve the problem of compactness, but could not achieve high magnetic fields and torques due to the fact that there is a lot of energy dissipation. There was a space between permanent magnets (PMs) of the superconducting coupling, which resulted in a low production of the magnetic field and torque. The secondary was composed of pellets, which the critical temperature is low. The fact that the critical temperature of the pellets was low, limited the operation and prevented it from reaching its maximum torque.

In a general dynamic application, a complete analytical procedure must be planned in order to optimally design a coupling according to the desired dynamics, and also considering the internal electromagnetic stresses of the coupling (i.e. PMs). Different analytical and numerical approaches have been adopted in studies on couplings [1], [16]–[19]. Even if precise, these different applications have some limitations. Numerical approaches take a long time. As for the analytical approaches, they rather offer flexible and precise solutions and, are therefore well suited to optimization designs in which the functions do not need to be differentiable [20], [21]. The limitations of the analytical methods are due to the fact that they are unable to take into account the PM coercivity and iron saturation (its permeability is considered to be infinity). Moreover, they do not allow to obtain the exact value of the thickness of the iron. Developed more recently [22]–[24], the magnetic equivalent circuit (MEC) is the method that we used because it is able to take into account material properties such as iron saturation, iron thickness, particle characteristics, i.e. both the remanence and coercivity, as well as the complex geometries, which are really important in achieving and obtaining better results.

As its main contribution, a novel hybrid superconducting coupling with axial-flux is developed and its torque characteristics are studied in this article using the magnetic circuit equivalent model. The main objectives of this study are to:

- Study the behavior of the superconductor material at high and low speed when it is associated with the conductor in a magnetic coupling under normal temperature and pressure conditions.
- Study the stability of the coupling at low and high speeds.
- Visualize the trajectories of the different lines of the magnetic fields and eddy currents.
- Determine the magnetic torque of the coupling when varying the thickness of the air gap and permanent magnets.
- Establish a magnetic equivalent circuit of the model, to obtain the results of the torque; in order to compare them with the results obtained by simulation.

Through this analysis and the methods used, we show that the coupling can work under normal temperature and pressure conditions.

III. RECENT FINDINGS

A. PROPOSED MODEL

The proposed coupling is showed in Figure 1, which consists of a primary and a secondary. The primary is made up of a steel disc in which PMs are mounted. The permanent magnets are axially magnetized and arranged alternately in the circumferential direction. The direction of N-pole magnets is positive while that of S-pole magnets is negative. The system consists of a mechanism that facilitates the rotation of half of the permanent magnets through an angle of 0 to 90 degrees. The magnet rotation mechanism is made up of a slip ring axis, driving shaft, big bevel gear, and a slip ring. The PMs are separated by small steel blades. As shown in Figure 1(c), the secondary is made up of a disc where are mounted the conductor and a superconductor. The superconductors at the secondary are separated by small steel blades. The blades that separate the conductor-superconductor assembly are initially used as housing for these different parts and also to prevent the latter from making movements during the rotation of the coupling. Taking into account that the thickness of the blades separating the conductor-superconductor assembly is very small compared to those of the conductor and the superconductor, its impact on the torque will be neglected. The conductor is made of copper and the superconductor is made of an alloy of Mercury, Rhenium, Barium, Calcium, copper, and oxide ($Hg_{0.8}Re_{0.2}Ba_2Ca_2Cu_3O_{8.8}$) [25] which its maximum critical temperature is 135 K and can operate under atmospheric pressure. The superconductor is Hi-shaped and wound on the surface of the copper core. During the winding process, the copper core is installed on the winding table for rotating motion, and each turn of the tape of the superconductor is soaked with two groups of Araldite resin to withstand low temperature environment. The components are bonded in the groove of the driving frame with the average radius of the groove. A cryogenic system with helium coolant is installed to be able to cool and regulate the temperature of the secondary of the coupling so that the operating temperature of the coupling never exceeds the superconductor critical temperature. As shown in figure 2 the cryogenic system is composed of a cryostat, cryostat lid and cryostat support. The secondary disk assembly is placed in the cryostat, the left end of the cryostat is fixedly connected with the cryostat lid by screws, and the lower end is installed on the cryostat support. The top of the cryostat has low and high temperature channels, and when the temperature of liquid helium in the thermostat reaches the critical temperature, the pump will extract the hot helium liquid inside the cryostat. The liquid helium extracted from the high-temperature

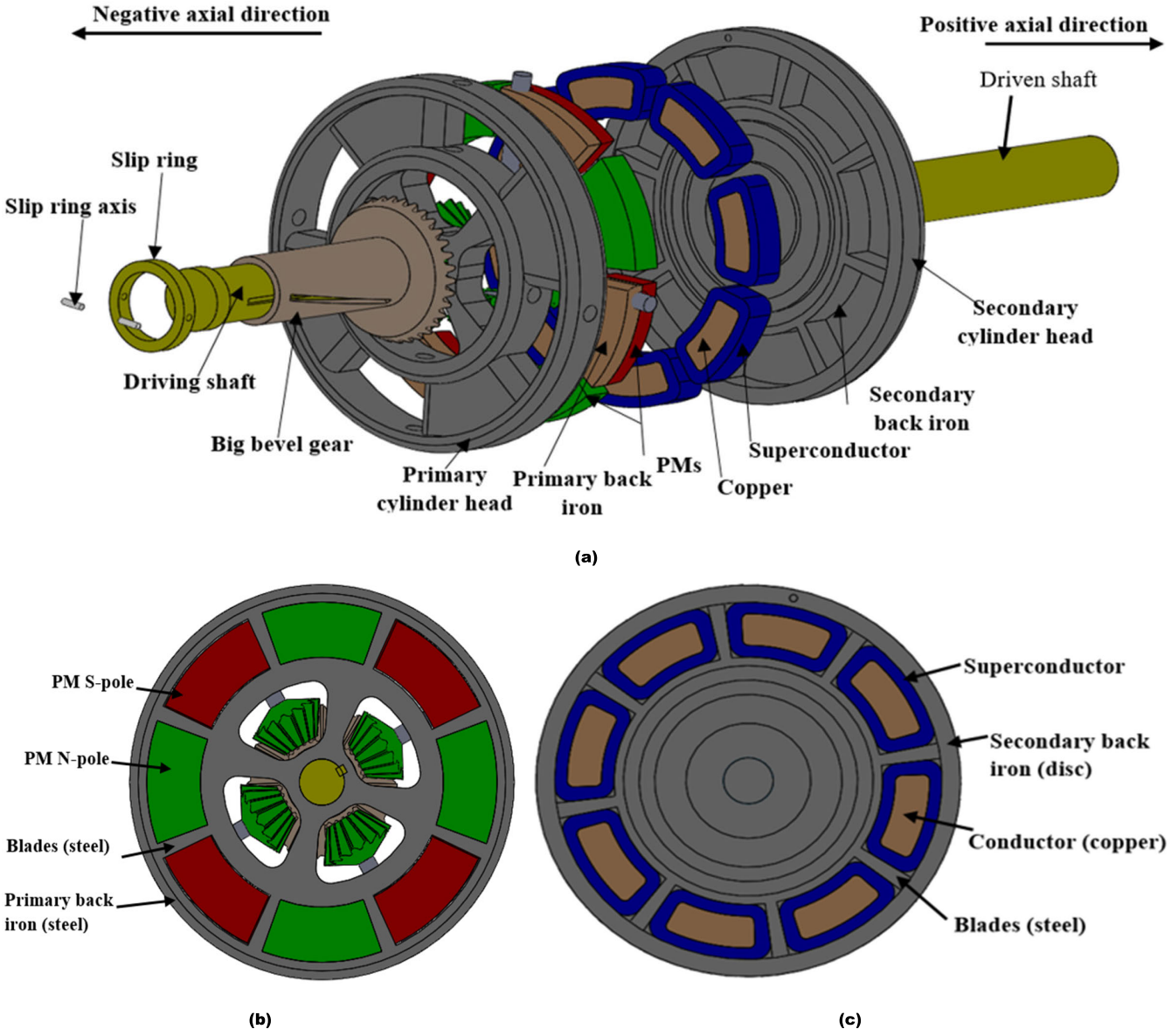

FIGURE 1. Schematic representation of the proposed model (a), the primary disk with PMs (b), the secondary disk with copper and superconductor (c).

channel is sent to the refrigerator for cooling. At the same time, the low-temperature liquid helium is input through the low-temperature channel to cool the superconductor, so as to ensure that the superconductor is always in a superconducting state during operation. The output speed of the coupling can be regulated by increasing or decreasing the air gap thickness or by rotating the S-pole permanent magnets from 0 to 90 degrees. The system is made up of permanent magnets that can rotate but throughout this paper we will first study the system only with the permanent magnets at 0 degree, i.e. the two disks are opposite (the permanent magnets and the conductor-superconductor assembly are placed face to face).

B. THEORY

Figure 3 shows the cross-section and geometrical parameters of the NHSC. The surface-mounted PMs axially-magnetized are alternately placed on the primary back iron. The conductor and the superconductor disks are embedded within the secondary back iron. We used the superconductor to trap the magnetic field in the air gap and avoid losses due to the joules effect. The magnetic field is trapped by the intermediary of the induced currents, resulting from the variation of the magnetic field applied to the superconductor. We also used the superconductor for screening. This magnetic field screening is based on the appearance of the induced current in the superconducting material. The appearance of these

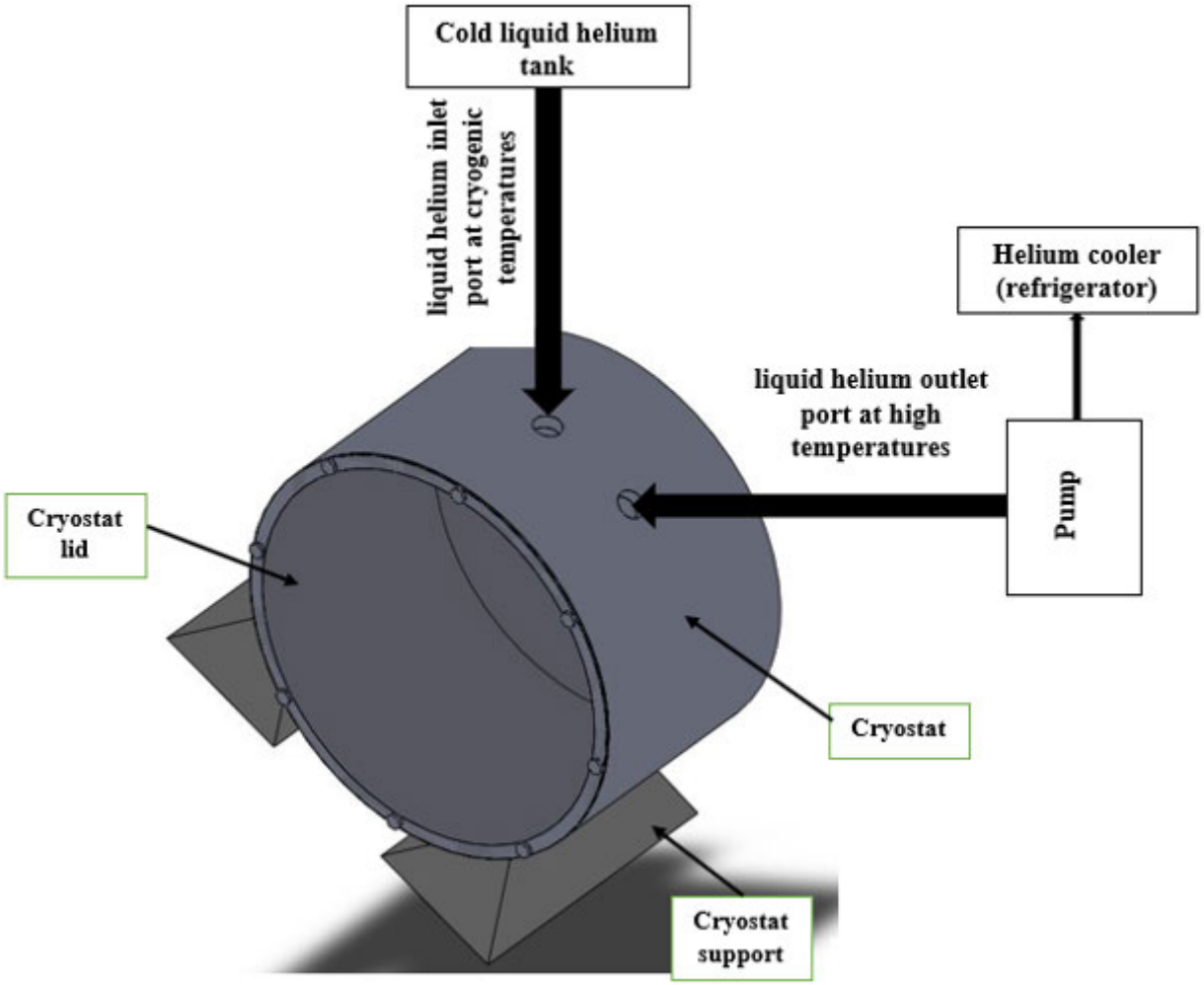

FIGURE 2. Cryostat.

currents will oppose the magnetic fields created at the PMs level; we will then observe a diamagnetic behavior of the superconductor. This superconductor faculty is implemented here to guide the magnetic field in the air gap or copper to end up with a large concentration of flux, and a considerable reduction in losses by the joules effect. Table 1 summarizes the specifications of the studied coupling.

1) BASIC ASSUMPTIONS AND 2D MODEL

To facilitate the calculation of eddy current and magnetic flux generated by the conductor disk during the movement, the coupling is expanded along with circumferential direction at the average length $r_m = (r_1 + r_2)/2$. Thus, the 3-D model is simplified to a 2-D model and we adopt the following reasonable assumptions.

1) The superconductor disk is always superconducting.
2) The superconductivity temperature of copper is far lower than that of the superconductor disk.
3) The relative permeability of the vacuum, PMs, superconductor, and conductor are μ_0, μ_{rm}, μ_{sc}, and μ_{rc} respectively, and $\mu_0 = 4\pi$e-07, $\mu_{rm} = 1.0997785406$, $\mu_{sc} = 0$, and $\mu_{rc} = 0.99991$.
4) The main magnetic flux passes vertically through the PMs, air gap, and conductor disk.
5) The thicknesses of the primary and secondary back iron are large enough to avoid magnetic saturation; thus, their permeabilities are considered to be infinite, and their reluctances are ignored.
6) The effect produced by the iron between the superconductor is neglected taking into account the fact that its thickness is very small compared to that of the superconductor and the conductor.

Different from the other magnetic couplings where the secondary was completely made up of conductors, the NHSC includes conductors and superconductors. The distribution of the magnetic field in NHSC is constantly changing during the movement. Therefore, a 2-D model is established based on the previous assumptions, as shown in Figure 3.

Figure 4(a) shows the magnetic circuit of the whole coupling. We note that the magnetic field is more important at the

TABLE 1. Parameters of the proposed NHSC.

Symbol	Description	value	Symbol	Quantity	value
h_m	Thickness of the PMs	10 mm	r_p	Inner radius of copper core,	78 mm
g	Air gap length	variable	r_n	Outer radius of copper core,	128 mm
h_c	Thickness of copper	10 mm	r_{mc}	Mean radius of the copper,	103 mm
h_{yp}	Primary yoke length	10 mm	N	Number of copper slots,	8
h_{ys}	Secondary yoke length	10 mm	Θ_c	Angle of the copper,	39°
Δh	Overhang length	3 mm	r_0	Outer radius of superconductor,	130 mm
r_2	Outer radius of the magnet	125 mm	h_{sc}	Thickness of the superconductor,	10 mm
r_1	Inner radius of the PMs	81 mm	Θ_{sc}	Angle of the superconductor,	44°
Θ_m	Angle of the PM	19°	σ_c	Conductivity of the copper,	58 MS
p	Number of pole of PMs	9		Material of yoke	Steel 1010
H_c	Coercivity of the PMs	-868 KA/m		Material of core	copper
	Electric field [25]	10 mv/m		Critical temperature [25]	135 K

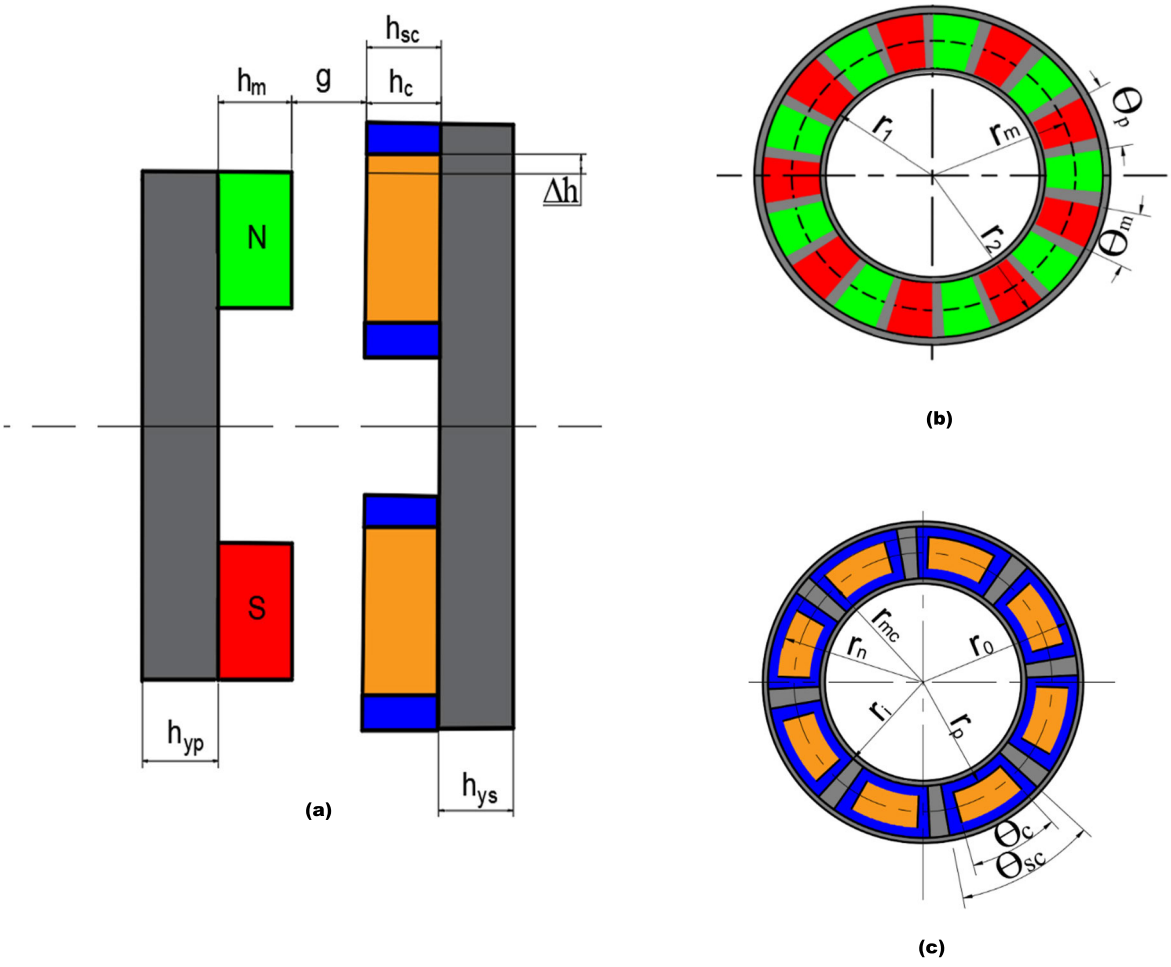

FIGURE 3. Geometry of an NHSC (a) 2D view of the NHSC (b) 2D view of the primary with PMs (c) 2D view of the secondary with superconductor disk.

contact surface between the adjacent permanent magnets. The magnetic field lines are uniform in the conductor and cross it forming loops. The magnetic field lines do not cross the superconductor and are repelled outwards. Figure 4(b) shows the leakages flux (dashed lines) and the magnetic flux paths (solid lines) in the primary, in the conductor disc, and the superconductor disk. The leakage flux (dashed lines) consists of three components: The first one is the leakage between the

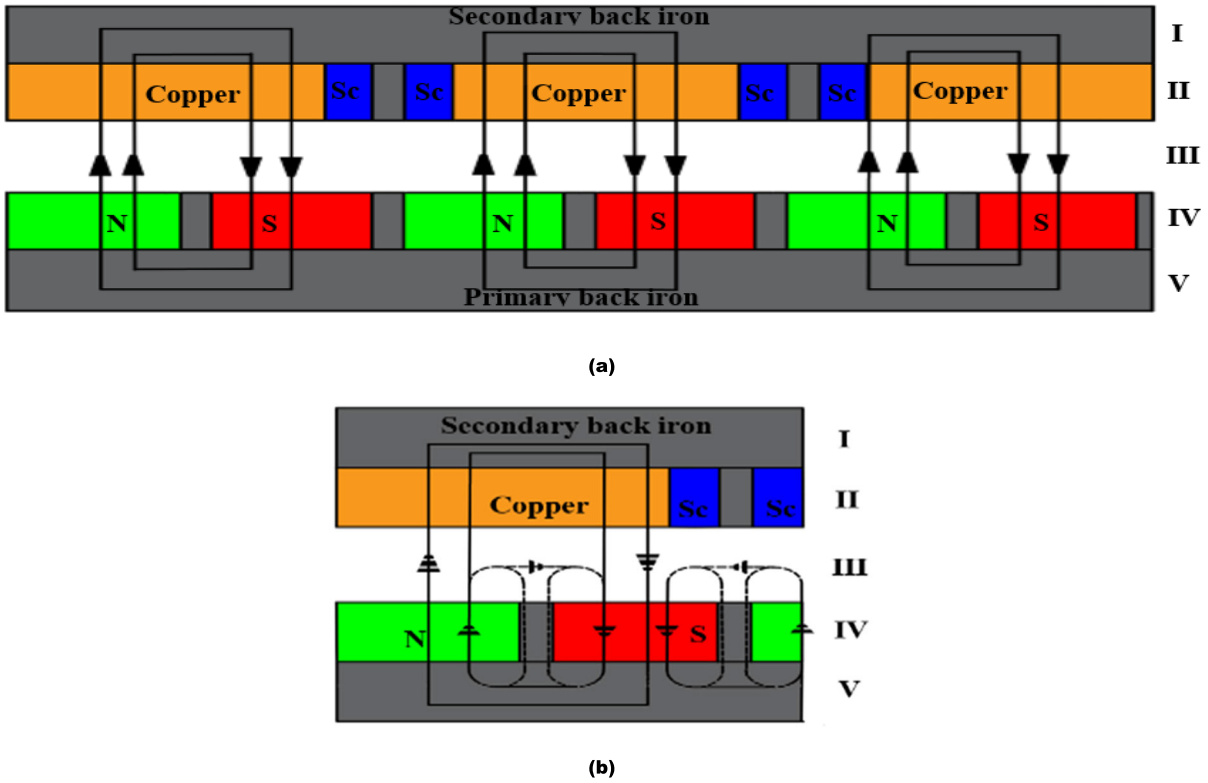

FIGURE 4. 2-D analytical model of NHSC (a) global, (b) section. (I: conductor and superconductor back iron; II: conductor and superconductor layer; III: air gap; IV: PM array; V: PM back iron).

adjacent PMs, the second is the leakage between the PMs and primary back iron and the third is the leakage flux between the adjacent PMs and the primary iron between them.

2) ESTABLISHMENT OF MEC MODEL

To establish the MEC model of the magnetic circuit, we analyze the magnetic flux paths and take into account only 50% of the pole pairs of the permanent magnets. Considering that the paths of the magnetic field of the NHSC are uniform and the reluctance of the superconductor is null, we establish an initial model of MEC, as shown in Figure 5. The permeability of the branch is zero if there is no branch at that position. The reluctance of the superconductor is zero since it is at the superconducting state. Considering the fact that the secondary is cooled, the reaction flux caused by the eddy current in the conductor and the superconductor is very low and therefore negligible. It should be noted that the model in Figure 5 is very complex and disadvantageous to analyze. As such, a simplified model is developed as shown in Figure 6 to ease calculation.

An equivalent 2D geometry is used by linearly expanding the scheme along with the average of the active part r_m. The pole pitch and the different mean arc lengths can be defined as follows:

$$\begin{cases} \tau_m = r_m \theta_m \\ \tau_c = r_{mc} \theta_c \\ \tau_p = 2\pi r_m / p \end{cases} \tag{1}$$

where τ_m and τ_p are the means pole arc lengths and the mean pole pitch of the PMs, τ_c is mean pole arc length of the conductor, and r_{mc} is the mean radius of the copper.

The magnetomotive force and reluctance of a PM can be given by the following

$$F_m = H_c h_m \tag{2}$$

$$R_m = \frac{h_m}{\mu_0 \mu_{rm} \tau_m (r_2 - r_1)} \tag{3}$$

The flux paths corresponding to the reluctance of leakage flux R_{mm} and R_{mi} have been drawn in Figure 5. We can see that the integration path of the leakage flux between adjacent PMs is composed of the straight-line segments inside PMs. The integration path of the leakage flux between the PMs and primary back iron includes a straight-line segment inside the PMs and a 1/2 arc of the air gap.

Therefore, the expressions of R_{mm}, and R_{mi} can be given by

$$R_{mi} = \frac{1}{\left(\frac{r_{mi}}{r_m} \times \frac{\mu_0 (r_2 - r_1)}{(1+\pi/2)}\right)} \tag{4}$$

$$R_{mm} = \frac{1}{\left(\frac{\mu_0 (r_2 - r_1)}{\pi}\right) ln\left(1 + \frac{\pi r_{mm}}{2h_m + \tau_p - \tau_m}\right)} \tag{5}$$

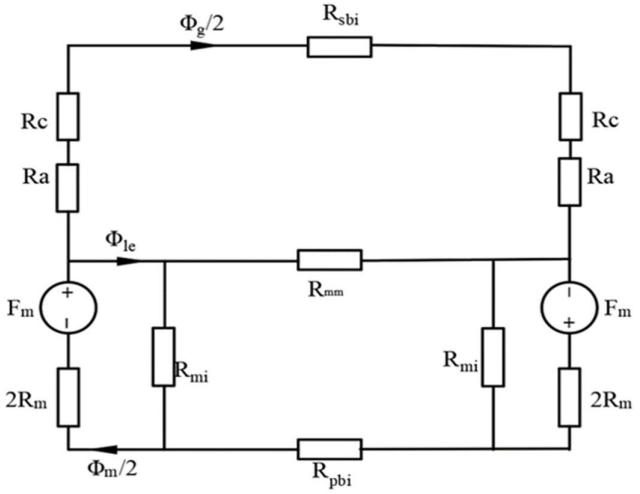

FIGURE 5. Initial MEC model.

The lengths of the integration paths r_{mm}, and r_{mi} are given according to the principle of minimum reluctance

$$r_{mm} = min\{g + h_c, \tau_m/2\} \tag{6}$$

$$r_{mi} = min\{g + hc, (\tau_p - \tau_m)/2\} \tag{7}$$

The reluctance R_{le} in Figure 4 is given by

$$R_{le} = R_{mi}//R_{mm}//R_{mi} \tag{8}$$

$$R_{le} = \frac{R_{mi} \times R_{mm}}{R_{mi} + 2R_{mm}} \tag{9}$$

The reluctance of the primary back iron and the secondary back iron can be given by

$$R_{pbi} = \frac{h_{yp}}{\mu_0 \tau_p (r_2 - r_1)} \tag{10}$$

$$R_{sbi} = \frac{h_{ys}}{\mu_0 \tau_p (r_2 - r_1)} \tag{11}$$

3) CALCULATION OF EDDY CURRENT REACTION EFFECT

a: FOR THE CONDUCTOR

The average magnetic field density of the area passing through the copper can be given by

$$B_{av} = \frac{\Phi_g}{\tau_m(r_2 - r_1)} \tag{12}$$

The average eddy current density of the conductor in the radial direction can be formulated as

$$J_{av} = \frac{\sigma_C \pi n_c r_m B_{av}}{30} \tag{13}$$

where n_c is the slip speed between the PMs and the superconductor disk.

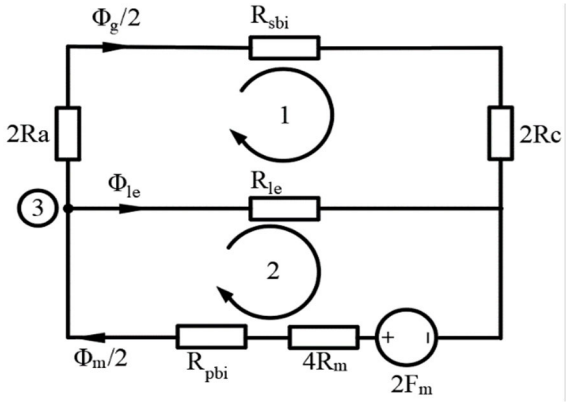

FIGURE 6. Simplified MEC Model.

b: FOR THE SUPERCONDUCTOR

The reluctance of the superconductor is null since it is at the superconductivity state. The resulting effect is that there is no resistance to the passage of eddy current. In theory, the model has a rotating magnetic field with the same rotational frequency. Therefore, the governing equations of the average magnetic field of the area around the superconductor disk are

$$\begin{cases} B_x = B_0 cos(\omega t) \\ B_y = B_0 sin(\omega t) \\ B_z = 0 \end{cases} \tag{14}$$

where B_0 is the amplitude of the static magnetic field, ω is the angular velocity of the rotating magnetic field, and t is the time.

According to FARADAY's law of electromagnetic induction, the spatially changing magnetic field inside the superconductor disk will induce an electric field, which can be given by:

$$\nabla \times E_i = -\frac{\partial B}{\partial t} \tag{15}$$

where E_i is the induced electric field and B is the magnetic field. When the rotational frequency of the magnetic field remains constant, or changes slowly, the change in the electric field over time is negligible. Therefore, the spatial distribution of the electric field can be obtained according to the AMPERE's law:

$$\begin{cases} \nabla \times H = J_i \\ J_i = \sigma_{sc} E_i \end{cases} \tag{16}$$

where σ_{sc} is the conductivity of the superconductor and J_i is the eddy current. As the temperature changes, the electrical conductivity of the superconductor will change accordingly.

4) EXPRESSIONS OF THE MAGNETIC FLUXES

Based on the MEC model shown in Figure 6, a matrix equation of magnetic fluxes can be established by applying Kirchhoff's law and this expression can be formulated

as follows:

$$\begin{pmatrix} 2R_m + \frac{R_{pbi}}{2} & R_{le} & 0 \\ 0.5 & -1 & -0.5 \\ 0 & R_{le} & -(R_a + R_c + \frac{R_{sbi}}{2}) \end{pmatrix} \times \begin{pmatrix} \phi_m \\ \phi_{le} \\ \phi_g \end{pmatrix} = \begin{pmatrix} 2F_m \\ 0 \\ 0 \end{pmatrix} \tag{17}$$

where ϕ_m, ϕ_{le} and ϕ_g are the magnetic flux through the PMs, the sum of the leakage flux between the adjacent PMs, the PMs and the back iron, and the air gap magnetic flux respectively.

By solving the matrix (17) and substituting the derivative equations, the different flux expressions can be written as follows:

$$\phi_g = \frac{4R_{le}F_m}{(2R_a+2R_c+R_{sbi})(R_{pbi}+R_{le}+4R_m)+R_{le}\left(4R_m+R_{pbi}\right)} \tag{18}$$

$$\phi_{le} = \frac{4(2R_a+2R_c+R_{sbi})F_m}{(2R_a+2R_c+R_{sbi})(R_{pbi}+R_{le}+4R_m)+R_{le}\left(4R_m+R_{pbi}\right)} \tag{19}$$

$$\phi_m = \frac{4F_m-2R_{le}\phi_{le}}{\left(4R_m+R_{pbi}\right)} \tag{20}$$

5) CALCULATIONS OF THE TORQUE

Although the eddy current is also generated by the iron teeth and back iron, the conductivity of the latter is very small compared to that of the copper and the superconductor disk, so the eddy current in the copper and the superconductor disk plays a dominant role. Since the resistance of the superconductor is zero, it pushes the magnetic field back to its surface and does not allow it to cross; so the magnetic field only crosses the copper conductor where the existence of an electromagnetic force only in places where the magnetic field crosses the conductor.

Considering the volume **V** occupied by one loop of the PMs, the corresponding traction force can be written as follows:

$$F = \int_v |J \times B| \, dV = k_s J_{av} B_{av} r_m (r_0 - r_i) h_{sc} \tag{21}$$

where k_s is the Russell-Norsworthy coefficient account-ting for the edge effect caused by the 3-D eddy current.

$$k_s = 1 - \frac{tanh\left[\pi L/2\tau_p\right]}{\left[\pi L/2\tau_p\right]\left\{1 + tanh\left[L/2\tau_p\right]\tanh\left(\pi\,\Delta h/2\tau_p\right)\right\}} \tag{22}$$

with $L = r_2 - r_1$

The electromagnetic torque of the coupling is

$$T = r_m \left(\sum_{n=1}^{2N} F_n\right) \tag{23}$$

where F_n is the traction force and n $=$ $1, 2, 3, \ldots, 16$, represent the number of the loops and N is the number of copper slots.

IV. RESULTS AND DISCUSSION

Figure 7 shows the simulation results of the flux and the magnetic field density of the NHSC. It can be observed that the main magnetic flux (solid lines) crosses the conductor but not the superconductor.

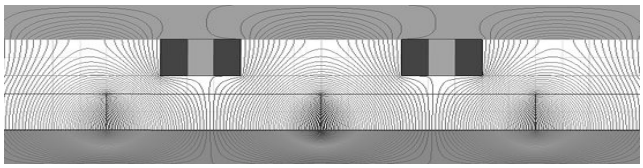

FIGURE 7. 2-D analytical model simulation of the NHSC.

We use a type II superconductor with a maximum critical temperature of 135 K, which gives a greater working margin compared to other superconductors. The operating temperature is fixed at 102 K. The curve of the evolution of the current density written as a function of the temperature of the superconductor is shown in Figure 8. To facilitate the calculations in our model, we have taken into consideration the value of the critical current density at 77 K, i.e., Jc $=$ $0.39 * 10^2$ A/cm^2 [25]. For 77 K to 135 K temperature range, the critical current density Jc was defined using 10 μV/mm as an electrical field criterion.

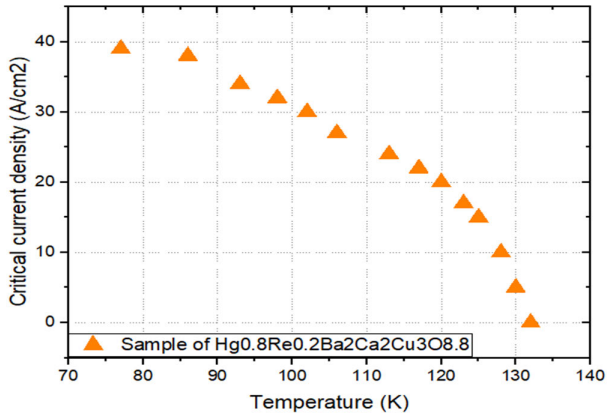

FIGURE 8. The critical current density Jc was defined using 10 μV/mm as electrical field criterion on a sample of $Hg_{0.8}Re_{0.2}Ba_2Ca_2Cu_3O_{8.8}$ [25].

The results obtained for this range of temperatures are summarized in Figure 8, 77 K represents the temperature in which the superconductor enters the vortex field zone, and 135 K represents the temperature above which the superconductor loses its superconductivity and therefore becomes a conductor.

To better understand where the hot spots are concentrated in the surface of the superconducting disk, Figure 9 illustrates the distribution of the eddy current at the surface of the superconducting disk when the coupling transmits maximum torque at a slip speed of 60 rpm. We can see in Figure 9 that

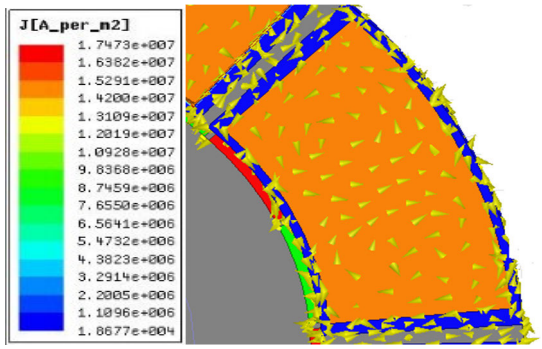

FIGURE 9. The distribution of the eddy current on the superconducting coupling.

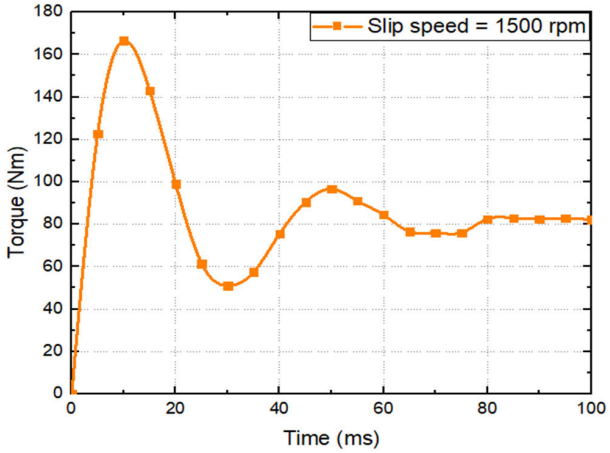

FIGURE 10. The torque versus time, slip speed = 1500 rpm, g = 2mm.

the distribution of the eddy current form two identical elliptical loops on each part of the conductor (copper); this is applied by the fact that the reluctance of the superconductor being zero, the eddy currents are maximum and concentrated on the conductor.

Figure 10 shows the curve of the torque with time when the slip speed is 1500 rpm. We can see that the torque can reach 167 Nm, which is very important in the domain of magnetic coupling. The fact that the superconducting coupling is composed of the superconductor and conductor, and also the zero resistivity of the superconductor allow the creation of a high-density magnetic field in the air gap; therefore, we can have a high torque transmitted.

Figure 11 shows the evolution of the torque as a function of time at different distances from the air gap. We can see that the swap has different values of the air gap. For a minimum air gap thickness, the torque can reach a value of almost 115 Nm. All the curves evolve in the same way, meaning that they reach the maximum peak and decrease, to end up being constant.

In Figure 12 we can see that when we increase the thickness of the PMs, the output torque decreases.

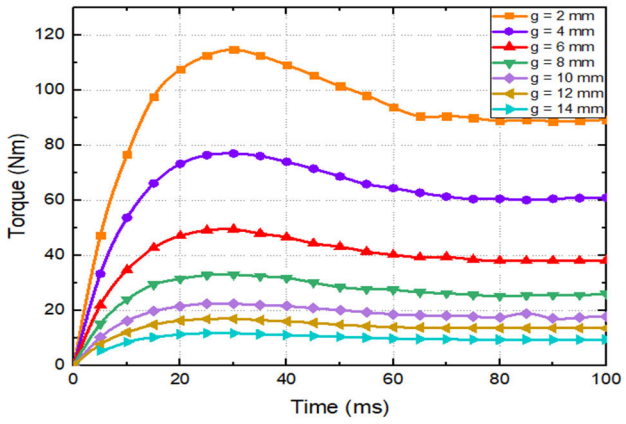

FIGURE 11. The torque versus the time at different air gap, slip speed = 60 rpm, h_m = 10 mm.

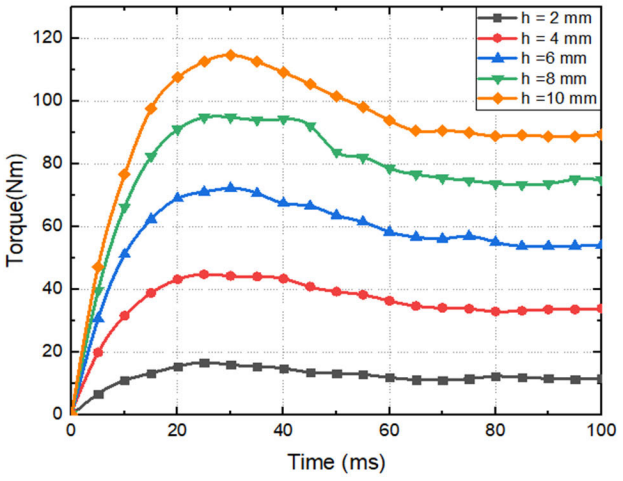

FIGURE 12. The torque versus the time at different thickness of PMs, slip speed = 60 rpm, g = 2 mm.

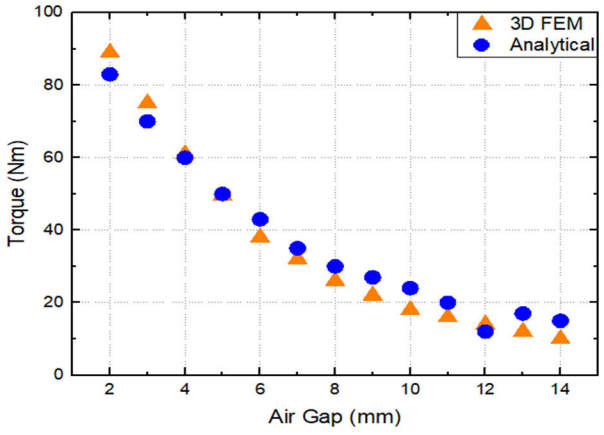

FIGURE 13. Torque versus air gap length, slip speed= 60 rpm, time = 100 ms.

As we can see in Figure 13, when the distance between the primary and the secondary of the coupling increases, the

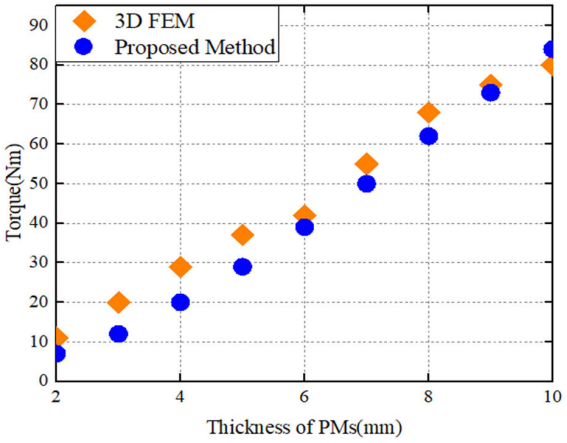

FIGURE 14. Torque versus thickness of the PMS, slip speed= 60 rpm, g = 2mm, time = 100 ms.

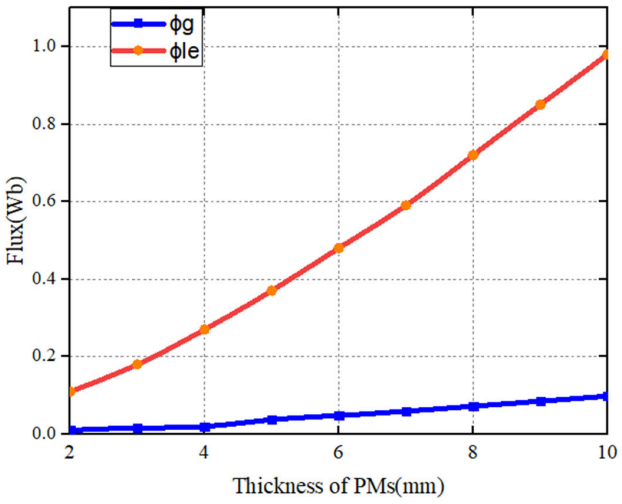

FIGURE 15. Flux versus thickness of the PMS, slip speed= 60 rpm, g = 2mm.

torque decreases. We can also see in the same figure that the curve representing the analytical values (obtained through the MEC model proposed) and the one representing the 3D finite element values are almost the same; which means that the model works well. The error is 6.74% when the air gap is 2 mm.

In Figure 14 when we increase slowly the thickness of the PMs, the torque also increases.

The 3D simulation results and the results obtained by the proposed MEC model are compared in Figure 13 and Figure 14 and they are almost the same. The same error between the two values is because we neglected some parameters, like by establishing the proposed MEC model, we considered that the reluctance of the superconductor is zero and taking into account the fact that the 3D-FEM does not allow a material with zero permeability, we set the value of this later close to zero. It is this small difference in value that is the consequence of this slight difference that we can visualize between the 3D-FEM and the proposed method. Based on the matrix (17) we obtained the different formulas of different fluxes using the proposed method. As we can see in Figure 15, the flow in the air gap increases according to the thickness of the PMs.

To obtain the curves, we have considered the constant slip speed at the value of 60 rpm and the thickness of the air gap is 2 mm. with the increase of the air gap thickness, we can see the flux between the air-gap increases slowly meanwhile the leakage flux increases exponentially.

V. CONCLUSION

In this paper, we have presented a new hybrid model of superconducting coupling. Our main objective was to know if by alternating the assembly superconductor conductor in the secondary of the coupling could function normally under normal temperature and pressure conditions. Through this research, it was found that when the conductor is surrounded by the superconductor, there is a reduction of losses by the joules effect. In this study, for the high critical temperature of the superconductor, the following findings were obtained:

- The stability of the superconductive coupling has been observed at high and low speeds, which validates the proposed model.
- The data presented showed that the torque peak at high speed could reach 167Nm and 115Nm at low speed.
- Increasing the air gap distance produces a decrease in electromagnetic torque while increasing the thickness of the PMs produces an increase of the electromagnetic torque.
- The eddy currents are maximal in the superconductor and minimal in the conductor and form two loops on the latter.
- The maximal error of 6.74% between the results calculated by the proposed model and the results obtained by the simulation were infinitely small, which validates the method used.

REFERENCES

[1] J. F. Charpentier, N. Fadli, and J. Jennane, "Study of ironless permanent magnet devices being both a coupling and an axial bearing for naval propulsion," *IEEE Trans. Magn.*, vol. 39, no. 5, pp. 3235–3237, Sep. 2003, doi: 10.1109/TMAG.2003.816732.

[2] X. Dai, Q. Liang, J. Cao, Y. Long, J. Mo, and S. Wang, "Analytical modeling of axial-flux permanent magnet eddy current couplings with a slotted conductor topology," *IEEE Trans. Magn.*, vol. 52, no. 2, pp. 1–15, Feb. 2016, doi: 10.1109/TMAG.2015.2493139.

[3] Z. Li, D. Wang, and D. Zheng, "Accurate prediction and analysis of electromagnetic fields and forces in flux-focusing eddy current coupling with double slotted conductor rotors," *IEEE Access*, vol. 6, pp. 37685–37699, 2018, doi: 10.1109/ACCESS.2018.2849857.

[4] P. Jin, Y. Tian, Y. Lu, Y. Guo, G. Lei, and J. Zhu, "3-D analytical magnetic field analysis of the eddy current coupling with Halbach magnets," *IEEE Trans. Magn.*, vol. 56, no. 1, pp. 10–13, Jan. 2020, doi: 10.1109/TMAG.2019.2950389.

[5] C. Yang, Z. Peng, J. Tai, L. Zhu, B. J. K. Telezing, and P. D. Ombolo, "Torque characteristics analysis of slotted-type eddy-current couplings using a new magnetic equivalent circuit model," *IEEE Trans. Magn.*, vol. 56, no. 9, pp. 1–8, Sep. 2020, doi: 10.1109/TMAG.2020.3009479.

[6] T. Lubin, S. Mezani, and A. Rezzoug, "Simple analytical expressions for the force and torque of axial magnetic couplings," *IEEE Trans. Energy Convers.*, vol. 27, no. 2, pp. 536–546, Jun. 2012, doi: 10.1109/TEC.2012.2183372.
[7] H. K. Razavi and M. U. Lampérth, "Eddy-current coupling with slotted conductor disk," *IEEE Trans. Magn.*, vol. 42, no. 3, pp. 405–410, Mar. 2006, doi: 10.1109/TMAG.2005.862762.
[8] W. K. Chu, K. B. Ma, C. K. McMichael, and M. A. Lamb, "Applications of high temperature superconductors on levitation bearings and other levitation devices," *Appl. Supercond.*, vol. 1, nos. 7–9, pp. 1259–1264, 1993, doi: 10.1016/0964-1807(93)90434-4.
[9] J. Zhu, Y. Zhao, P. Chen, S. Jiang, S. Wang, J. Fang, X. Zhao, and H. Wang, "Magneto-thermal coupling design and performance investigation of a novel hybrid superconducting fault current limiter (SFCL) with bias magnetic field based on MATLAB/SIMULINK," *IEEE Trans. Appl. Supercond.*, vol. 29, no. 2, pp. 1–5, Mar. 2019, doi: 10.1109/TASC.2019.2892295.
[10] W. Meissner and R. Ochsenfeld, "Ein neuer effekt bei eintritt der Supraleitfähigkeit," *Die Naturwissenschaften*, vol. 21, no. 44, pp. 787–788, Nov. 1933, doi: 10.1007/BF01504252.
[11] Q. Hu, X. Wang, M. Guan, and Y. Zhou, "Magneto-mechanical coupling analysis of a superconducting solenoid using FEM with different approaches," *IEEE Trans. Appl. Supercond.*, vol. 30, no. 4, Jun. 2020, Art. no. 4900305, doi: 10.1109/TASC.2020.2969402.
[12] P. Yang, S. Dai, T. Ma, J. Huang, G. Jiang, Y. Wang, Z. Hong, and Z. Jin, "Analysis of peak electromagnetic torque characteristics for superconducting DC induction heaters," *IEEE Access*, vol. 8, pp. 14777–14788, 2020, doi: 10.1109/ACCESS.2019.2963718.
[13] D. Castelvecchi, "Room-temperature superconductor puzzles physicists," *Nature*, vol. 586, no. 7829, p. 349, 2020.
[14] E. Snider, N. Dasenbrock-Gammon, R. McBride, M. Debessai, H. Vindana, K. Vencatasamy, K. V. Lawler, A. Salamat, and R. P. Dias, "Room-temperature superconductivity in a carbonaceous sulfur hydride," *Nature*, vol. 586, no. 7829, pp. 373–377, Oct. 2020, doi: 10.1038/s41586-020-2801-z.
[15] P. Tixador, P. Hiebel, E. Hotier, X. Chaud, and E. Beaugnon, "Superconducting coupling device," *Cryogenics*, vol. 35, no. 9, pp. 567–572, 1995, doi: 10.1016/0011-2275(95)91255-J.
[16] A. Canova and B. Vusini, "Analytical modeling of rotating eddy-current couplers," *IEEE Trans. Magn.*, vol. 41, no. 1, pp. 24–35, Jan. 2005, doi: 10.1109/TMAG.2004.839730.
[17] J. Wang and J. Zhu, "A simple method for performance prediction of permanent magnet eddy current couplings using a new magnetic equivalent circuit model," *IEEE Trans. Ind. Electron.*, vol. 65, no. 3, pp. 2487–2495, Mar. 2018, doi: 10.1109/TIE.2017.2739704.
[18] S. Mohammadi, M. Mirsalim, S. Vaez-Zadeh, and H. A. Talebi, "Analytical modeling and analysis of axial-flux interior permanent-magnet couplers," *IEEE Trans. Ind. Electron.*, vol. 61, no. 11, pp. 5940–5947, Nov. 2014, doi: 10.1109/TIE.2014.2311391.
[19] A. S. Erasmus and M. J. Kamper, "Computationally efficient analysis of double PM-rotor radial-flux eddy current couplers," *IEEE Trans. Ind. Appl.*, vol. 53, no. 4, pp. 3519–3527, Jul. 2017, doi: 10.1109/TIA.2017.2690986.
[20] B. N. Cassimere and S. D. Sudhoff, "Population-based design of surface-mounted permanent-magnet synchronous machines," *IEEE Trans. Energy Convers.*, vol. 24, no. 2, pp. 338–346, Jun. 2009, doi: 10.1109/TEC.2009.2016150.
[21] J. A. Krizan and S. D. Sudhoff, "A design model for salient permanent-magnet machines with investigation of saliency and wide-speed-range performance," *IEEE Trans. Energy Convers.*, vol. 28, no. 1, pp. 95–105, Mar. 2013, doi: 10.1109/TEC.2012.2223699.
[22] S. Mohammadi and M. Mirsalim, "Double-sided permanent-magnet radial-flux eddy-current couplers: Three-dimensional analytical modelling, static and transient study, and sensitivity analysis," *IET Electr. Power Appl.*, vol. 7, no. 9, pp. 665–679, Nov. 2013, doi: 10.1049/iet-epa.2013.0050.
[23] S. Mohammadi, M. Mirsalim, and S. Vaez-Zadeh, "Nonlinear modeling of eddy-current couplers," *IEEE Trans. Energy Convers.*, vol. 29, no. 1, pp. 224–231, Mar. 2014, doi: 10.1109/TEC.2013.2288948.
[24] S. Mohammadi and M. Mirsalim, "Design optimization of double-sided permanent-magnet radial-flux eddy-current couplers," *Electr. Power Syst. Res.*, vol. 108, pp. 282–292, Mar. 2014, doi: 10.1016/j.epsr.2013.11.014.
[25] M. T. D. Orlando, V. A. Rodrigues, S. P. Dias, J. F. Fardin, D. S. L. Simonetti, H. Belich, C. C. Carvalho, J. L. D. S. Neto, E. S. Yugue, and M. M. Werneck, "$Hg_{0.8}Re_{0.2}Ba_2Ca_2Cu_3O_{8.8}$ thick film produced by laser ablation," *J. Microw., Optoelectron. Electromagn. Appl.*, vol. 10, no. 1, pp. 114–120, Jun. 2011, doi: 10.1590/S2179-10742011000100012.

BORIS JOEL KENNE TELEZING received the B.Sc. degree from the University Institute of Technology, Cameroon, in 2013, and the M.Sc. degree from the University Institute of the Coast, Cameroon, in 2016. He is currently pursuing the Ph.D. degree with Jiangsu University. He was a Maintenance Technician with Guinness Diageo. His current research interests include magnetic fields, eddy currents, and superconductors.

CHAOJUN YANG received the M.Sc. and Ph.D. degrees from Jiangsu University, Zhenjiang, China, in 1997 and 2013, respectively. She is currently a Professor and a Ph.D. Supervisor with the School of Mechanical Engineering, Jiangsu University. Her current research interests include the analysis and design of magnetic drive machines, laser processing technology, mechanical transmission.

PATRICK DJOMO OMBOLO received the B.Sc. degree from the University of Douala, Cameroon, in 2012, and the M.Sc. degree from the University of Ngaoundere, in 2014. He is currently pursuing the Ph.D. degree with Jiangsu University. His current research interests include computation of magnetic fields, eddy currents, and electromagnetic performance prediction of permanent-magnet machines.

ZHIZHUO PENG received the B.Sc. degree from Shenyang Ligong University, Shenyang, China, in 2018, and the M.Sc. degree from Jiangsu University, China, in 2021. His research interests include computation of magnetic fields, eddy currents, and electromagnetic performance prediction of permanent-magnet machines.

JIANGXI TAI received the B.Sc. degree from the Taiyuan University of Science and Technology, Taiyuan, China, in 2018, and the M.Sc. degree from Jiangsu University, China, in 2021. His research interests include computation of magnetic fields, eddy currents, and electromagnetic performance prediction of permanent-magnet machines.

LI ZHU received the B.Sc. degree from the Jiangsu Institute of Technology, Changzhou, China, in 2018, and the M.Sc. degree from Jiangsu University, China, in 2021. Her research interests include computation of magnetic fields, eddy currents, and electromagnetic performance prediction of permanent-magnet machines.